Fracture analysis of outcrop analogues to support modelling of the subseismic domain in carbonate reservoirs, south-central Pyrenees

JON GUTMANIS[1,2]*, LLUÍS ARDÈVOL I ORÓ[2,3], DAVINIA DÍEZ-CANSECO[2,4], LYNDA CHEBBIHI[1], ABDULLAH AWDAL[1] & ALEXANDER COOK[1]

[1]*GeoScience Ltd, Falmouth Business Park, Bickland Water Road, Falmouth, Cornwall TR11 4SZ, UK*

[2]*Catalonia Geological Research, 25620 Tremp, Catalonia, Spain*

[3]*Geoplay Pyrenees Ltd, 6 Nerets, 25630 Talarn, Catalonia, Spain*

[4]*Departamento de Estratigrafía, Universidad Complutense de Madrid-IGEO, 2 José Antonio Novais, 28040 Madrid, Spain*

Correspondence: Gutmanis@geoscience.co.uk

Abstract: The productivity of wells in fractured reservoirs depends, in terms of rate and sustainability, on the heterogeneity and variable connectivity of the open fracture network. Outcrop studies in Cretaceous carbonates from the Catalan Pyrenees illuminate this issue and reveal the degree of uncertainty associated with the interpretation of fracture data from wells and seismic. Three examples are chosen to provide verifiable data, parameters and concepts which can be applied to the workflow of fractured reservoir characterization. We discuss fracture properties and distributions in the subseismic volume, the coupled behaviour between litho-mechanical properties, *in situ* stress and fracturing, and the permeability properties of fault damage zones. The outcrops also highlight some of the difficulties involved in constructing static reservoir models and evaluating fracture interpretations derived from software-based techniques such as surface curvature.

Fractured reservoirs where storage and/or well performance depend on a well-connected open fracture system (Types 1 and 2 of Nelson 2001) include several rock types such as tight limestones and dolomites, low-porosity clastic deposits, especially Palaeozoic quartzites, volcanic rocks and basement formations ranging from igneous to metamorphic. In recent years many operating companies have set out to identify and map the properties and distribution of reservoir fracture systems in order to evaluate reservoir quality and model performance. Some representative studies have been published (e.g. Nelson *et al.* 2000; Gouth *et al.* 2006; Fonta *et al.* 2007; Souche *et al.* 2012). In addition, numerous outcrops have been studied as analogues for the subsurface, ranging from the North Sea chalk (e.g. Welch *et al.* 2015) to the Mesozoic and Cenozoic carbonates of the Zagros (e.g. Wennberg *et al.* 2006; Stephenson *et al.* 2007; Casini *et al.* 2011), the Pyrenees (e.g. Shackleton *et al.* 2005, 2011; Tavani *et al.* 2011) and the Apennines (e.g. Aydin *et al.* 2010). A review of this large volume of open-source material, with emphasis on foreland basins and fold-and-thrust belts, was recently published by Tavani *et al.* (2015).

Most fractured reservoirs show large variations in open fracture intensity, orientation and connectivity. This heterogeneity can have a significant impact on the distribution of reservoir quality and sustainability of production (e.g. Casini *et al.* 2011). Another important attribute is fracture dimension. In our experience, the term 'fracture' is often used in reservoir appraisal to embrace everything from micro- to meso- or even macro-scale structures. Precision is needed in defining fracture type and associated dimension because length and aperture tend to correlate and, when coupled with a range of fracture orientations, longer length increases fracture connectivity. In fact, inflow to wells is often better correlated with single large-aperture fractures than with high fracture intensity (Narr *et al.* 2006). This reflects the so-called 'cubic law', which states that flow is proportional to the cube of aperture for parallel-plate flow (see Klimczak *et al.* 2010 for a review of many previous papers on the topic).

In this paper we consider the following hierarchy of fracture scale (Table 1):

(a) background fracture system (metre-scale), generally bed-limited (stratabound) fractures

Table 1. *Fracture types and scale hierarchy*

Approximate length/height scale (m)	Hierarchy term	Fracture type examples	Most relevant data type for their identification
<0.20	Micro-scale	Most stylolites, tension gash veins, 'hairline' fractures	Core
0.20–10	Meso-scale	Regional or fold-related joint systems, fault-related fractures	Core, image logs, full waveform sonic
10–200	Meso- to macro-scale (the 'seismic gap')	Fracture 'corridors' and subseismic faults with <10 m throw (see text discussion)	High-resolution seismic processed for fracture-related attributes
200–1000	Macro-scale	Seismic-scale faults	3D seismic and other geophysical datasets

of *c.* 0.1–1 m height depending on bed thickness;

(b) fracture corridors (meso-scale), linear zones of high fracture intensity of tens to hundreds of metres in dimension;

(c) subseismic-scale faults (meso- to macro-scale), below seismic resolution but sometimes identifiable in attribute maps (for the purposes of this study we take a fault throw of 10 m as the limit of seismic resolution, although this is dependent on several factors especially bed thickness v. seismic wavelength; e.g. Arthur *et al.* 2015); and

(d) seismic-scale faults (macro-scale).

Fracture types and their key attributes are normally mapped and quantified during reservoir appraisal. However, both well and seismic data have limitations when it comes to mapping meso-scale fractures such as fracture corridors. These generally exist below the limit of seismic resolution, although seismic attribute analyses may help (e.g. Fonta *et al.* 2007; Singh *et al.* 2008; Souche *et al.* 2012). Borehole image logs and core are also of limited assistance. The distribution of meso-scale fractures is often heterogeneous (Casini *et al.* 2011; Sassi *et al.* 2012) and unpredictable and, unlike metre-scale fractures, whose height is generally related to stratigraphy (e.g. Couples *et al.* 1998; Wennberg *et al.* 2006; Laubach *et al.* 2009), it is unclear whether the same relation holds true for fracture corridors. However, well test data, outcrop (Ogata *et al.* 2014) and analogue studies (Belayneh *et al.* 2007) show that the impact of meso-scale fractures on fluid flow and connectivity can be very significant (e.g. Fonta *et al.* 2007; Souche *et al.* 2012).

Outcrop studies can mitigate these problems by providing visualization for seismic and well data and generating parameters and concepts which serve to control reservoir modelling. We describe some specific outcrops in Upper Cretaceous carbonates of the Pyrenees fold-and-thrust belt with this is mind. The following themes are discussed, all of them in the context of carbonate host rocks exposed at outcrop:

(a) at Aramunt (outcrop A, Fig. 1), we describe the challenge of capturing fracture heterogeneity across the hierarchy of scale from seismic to subseismic;

(b) at Hortoneda (outcrop H), we discuss the benefits of evaluating the coupled relationship between *in situ* stress, mechanical anisotropy and fracture distribution; and

(c) at Bóixols (outcrop B), we assess the common assumption that fault damage zones are always good targets for exploration or production wells.

Geological setting

The Pyrenees are an Alpine orogen extending east to west along the northern margin of the Iberian peninsula (Fig. 1a), formed during Late Cretaceous–Miocene time as the Iberian and European plates collided (Choukroune & ECORS Pyrenees Team 1989). The central Pyrenees have a fan-like geometry with an axial antiformal stack of mostly Hercynian basement rocks, flanked by both north- and south-directed Mesozoic–Eocene fold-and-thrust units detached above Triassic evaporites (Muñoz 1992). The South-Central Pyrenean thrust unit (Séguret 1972) consists of a piggy-back imbricate sequence of three thin-skinned thrust sheets (Vergés & Muñoz 1990). The three outcrops studied in this paper are located within the oldest and uppermost of these structures, the Bóixols thrust sheet.

The Bóixols thrust sheet can be traced for 40 km along the eastern sector of the South-Central Pyrenean thrust unit (Berástegui *et al.* 1990), widening from east to west to reach 14 km in its central part, before plunging westwards below younger
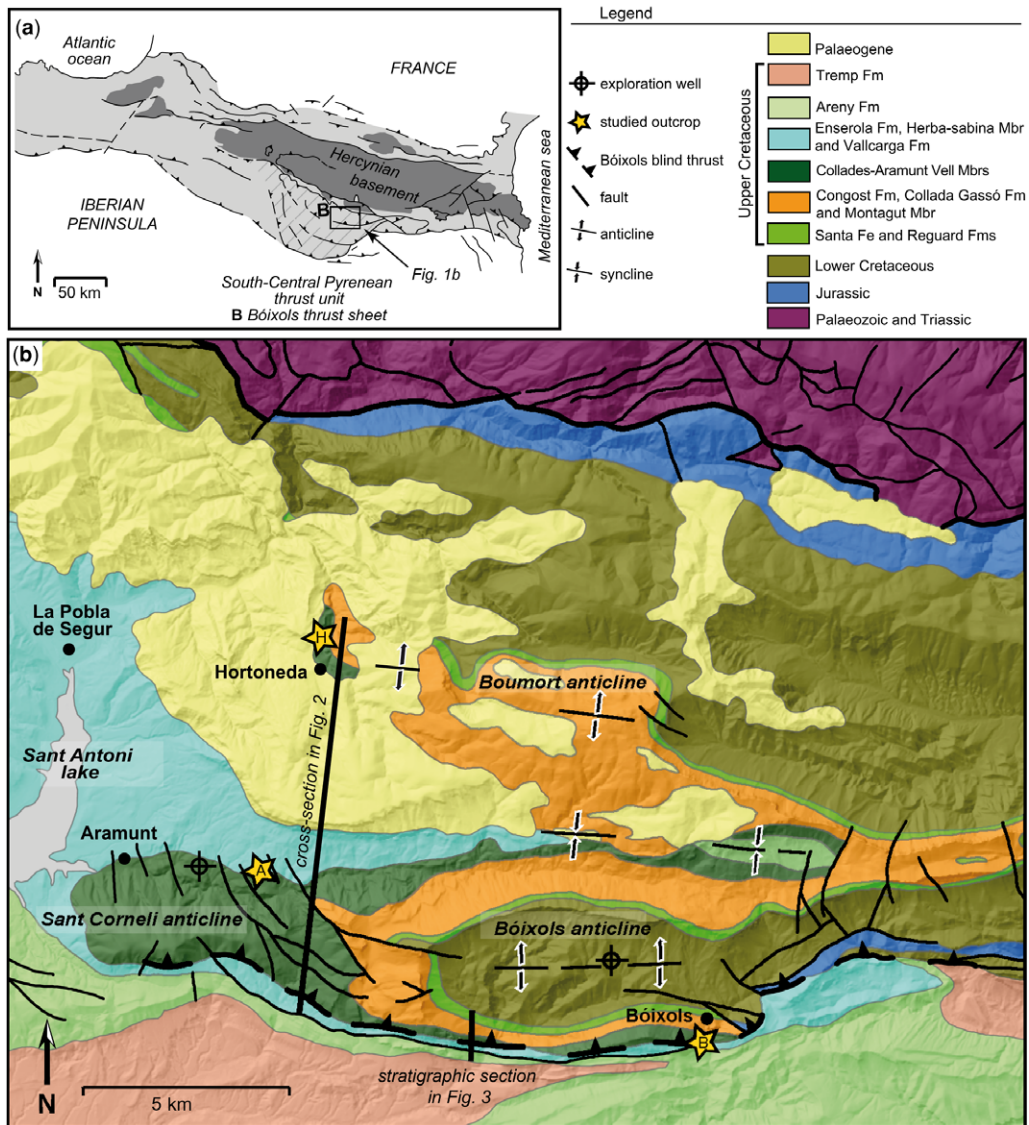
Fig. 1. Geological setting of the studied outcrops. (**a**) Tectonic map of the Pyrenees showing the location of the study area in the South-Central Pyrenean thrust unit. (**b**) Geological map of the central part of the Bóixols thrust sheet with location of the outcrops, the structural cross-section (Fig. 2) and the general stratigraphic section (Fig. 3).

sediments (latest Cretaceous) (Fig. 1). The Mesozoic carbonates of the Bóixols sheet are affected by three east–west-trending complex folds: the Sant Corneli-Bóixols and Boumort anticlines where the Aramunt and Hortoneda outcrops are located, respectively, linked by an intermediate syncline (Figs 1b & 2) (Mencos *et al.* 2015).

The Sant Corneli-Bóixols anticline is an asymmetrical fold with a backlimb dipping about 30°N and a subvertical to overturned southern forelimb,

in the hanging wall of an inferred south-directed Bóixols blind thrust. Detailed structural descriptions are provided by Mencos *et al.* (2011), Shackleton *et al.* (2011) and Tavani *et al.* (2011). The anticline is assumed to have formed by oblique inversion of Lower Cretaceous extensional structures and propagation of the Bóixols thrust during Late Cretaceous time (Berástegui *et al.* 1990; Bond & McClay 1995; Garcia-Senz 2002; Mencos *et al.* 2015). The Bóixols outcrop is located in a north-dipping reverse
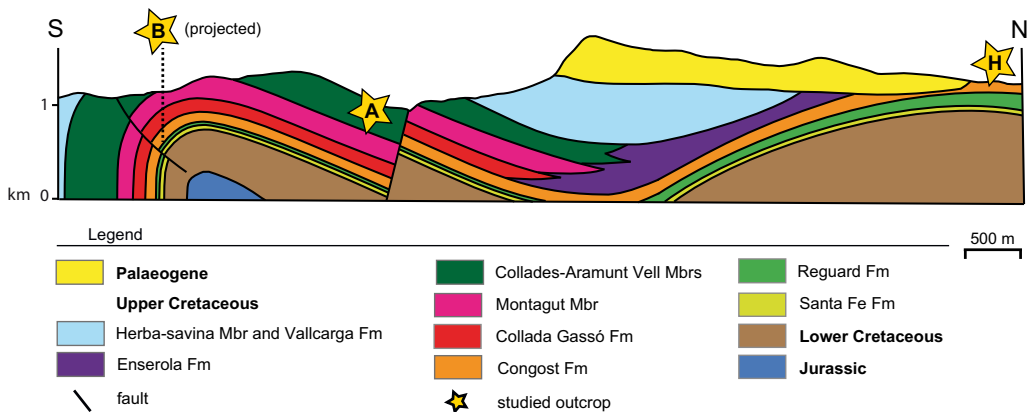
Fig. 2. Surface cross-section of the Bóixols thrust sheet, modified and simplified from Muñoz *et al.* (2010), with location of the studied outcrops.

fault that cuts the Upper Cretaceous section in the hanging wall of the Bóixols thrust (Fig. 2).

The outcrops occur within the Late Cenomanian–Santonian interval, classically interpreted as a post-rift sequence that was deposited prior to the Alpine compression (Puigdefàbregas & Souquet 1986; Muñoz 1992). Formations and members are as defined by Mey *et al.* (1968), Gallemí *et al.* (1982), Vicens *et al.* (1998) and Skelton *et al.* (2003).

The Upper Cenomanian Santa Fe Formation is rather uniform and consists of shelfal limestones (Fig. 3). They are sharply overlain by deeper-water Turonian marls (Reguard Formation) which increase in thickness from south to north and grade upwards to Turonian–Coniacian reefal carbonates (Congost Formation). The Hortoneda outcrop encompasses the upper part of the Reguard Formation and the Congost Formation, which in turn is successively overlain by the Coniacian–Santonian Collada Gassó, Montagut and Collades–Aramunt Vell lithostratigraphic units and lateral equivalents. These units consist of alternating brown cross-bedded clastic grainstones and rudist-rich carbonates, distally grading to nodular marls. The Aramunt outcrop is located in the middle part of the Aramunt Vell unit, while the Bóixols outcrop encompasses thrusted rocks of Late Cenomanian–Coniacian age (Santa Fe to Collada Gassó formations).

## Aramunt: characterizing the subseismic volume

In the north limb of the Sant Corneli anticline, a few kilometres east of Aramunt village and south of the 'Vilanoveta trenches', the east–west-striking canyon wall exposes a continuous sequence of Coniacian–Santonian shelf margin carbonates of the Aramunt Vell member (Fig. 4a). The lower part of the sequence comprises eight coarsening upwards parasequences (Fig. 4b, d); the lower four are marly nodular limestones capped by cross-bedded sandy grainstones, and the upper four are rudist-coral limestones, massive and relatively competent (Vicens *et al.* 1998; Pomar *et al.* 2005). The grainstones are competent but have much internal cross-bedding, while the marly limestones are relatively weak and ductile. This range of lithologies imparts a significant litho-mechanical anisotropy which has a direct influence on the fracture system.

The exposure is cut by bed-scale stratabound fractures, non-stratabound fracture corridors, and subseismic- to seismic-scale faults. The subseismic faults are generally normal to oblique-normal and have displacements of up to 10 m. This type of fracture-scale hierarchy is commonly identified and inferred from analysis of well and seismic data in reservoirs. However, most of the fracture system in the Aramunt outcrop is well below seismic scale, illustrating the challenge faced in reservoir appraisal (Fig. 5).

Orientation and spacing data of more than 700 fractures of all types were collected along three 500 m long scan-lines between major faults F2 and F3 (Figs 4b, d & 6). Aperture data were not collected because of likely enhancement by near-surface stress relief and weathering processes. The data reveal a dominant NNW–SSE strike for faults, fracture corridors and background fractures alike, sub-parallel to the seismic-scale faults observed in the backlimb of the Sant Corneli anticline (Fig. 1b). A subsidiary north–south to NNE–SSW trend is interpreted as a weaker conjugate fracture set. These trends are consistent with previous studies (Shackleton *et al.* 2011; Tavani *et al.* 2011).
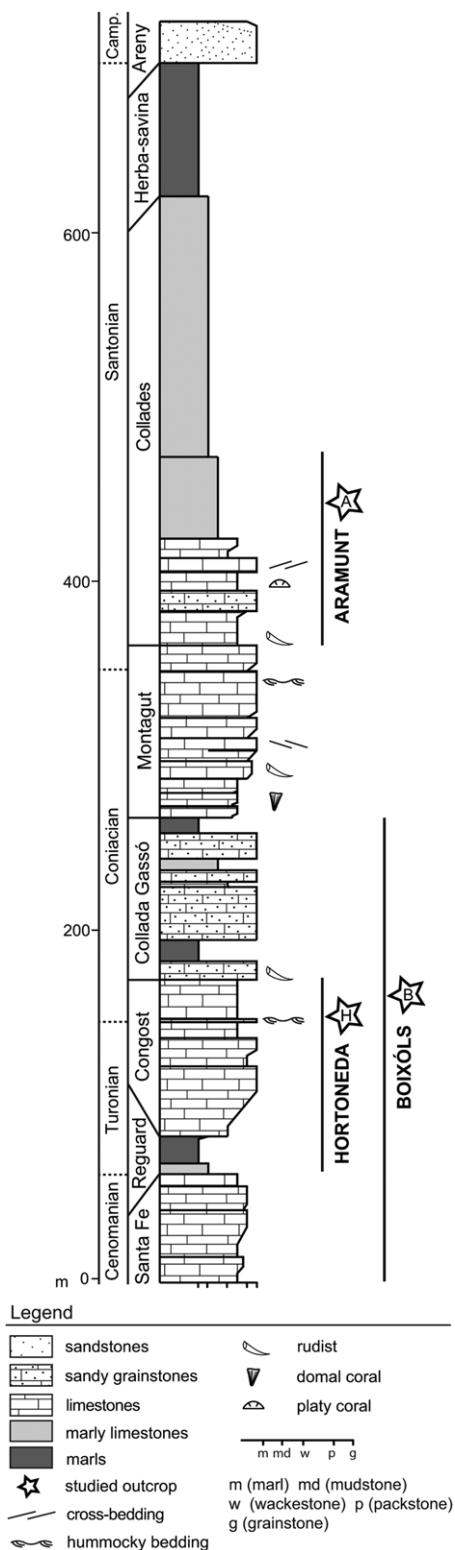
Based on field relations, Tavani *et al.* (2011) interpreted the dominant NNW–SSE metre-scale structures as extensional fractures due to early NNW–SSE-directed layer-parallel shortening immediately prior to the onset of fold growth. In contrast, Shackleton *et al.* (2011) interpreted them as syn-fold growth extensional structures. The current work reported here does not set out to distinguish between these interpretations; however, we do note the regular distribution of the NNW–SSE fractures and the common occurrence of calcite mineralization. These observations suggest systematic fracturing in a burial environment of high pore pressure, implying onset of layer-parallel shortening and early stages of inversion.

Modelling the background fracture system

Spacings and dimension of the Aramunt background fracture system are largely controlled by mechanical layering, a geometry consistent with many studies of bed-thickness–fracture-spacing relationships (e.g. Cooke & Underwood 2001; Wennberg *et al.* 2006). In reservoir characterization, background fracture systems are typically sampled by image logs, providing spacing and orientation statistics to construct static fracture models. To provide an analogue, the Aramunt scan-line data have been used to build a discrete fracture network (DFN) model in RMS software (Emerson Roxar) (Fig. 7). The model was scaled up and used for porosity modelling (Fig. 7c). Porosity broadly correlates with the intensity of the background fracture system, increasing towards F3 especially in its footwall. Higher porosities are associated with the fracture damage zone of F3. Although simple, the exercise enables the predictive capabilities of the software to be tested.

### The fracture corridors and subseismic faults

It is likely that only faults F2 and F3, spaced 465 m apart, have sufficient displacement to be seen on seismic profiles (indicated as SF on the pseudo-seismic profile in Fig. 4c). The subseismic faults (SSF) and fracture corridors (FC) that occur between F2 and F3 can be inferred to have lengths measured in tens of metres, and therefore might be seen as subtle lineaments in seismic attribute maps such as those shown in Singh *et al.* (2008). In some reservoir appraisals, lineaments and edge features such as dip similarity are assumed to be SSF and/or FC

Fig. 3. Stratigraphic section of the southern limb of the Sant Corneli anticline showing formal geological formations and members and their ages (Mey *et al.* 1968; Gallemí *et al.* 1982; Vicens *et al.* 1998; Skelton *et al.* 2003).
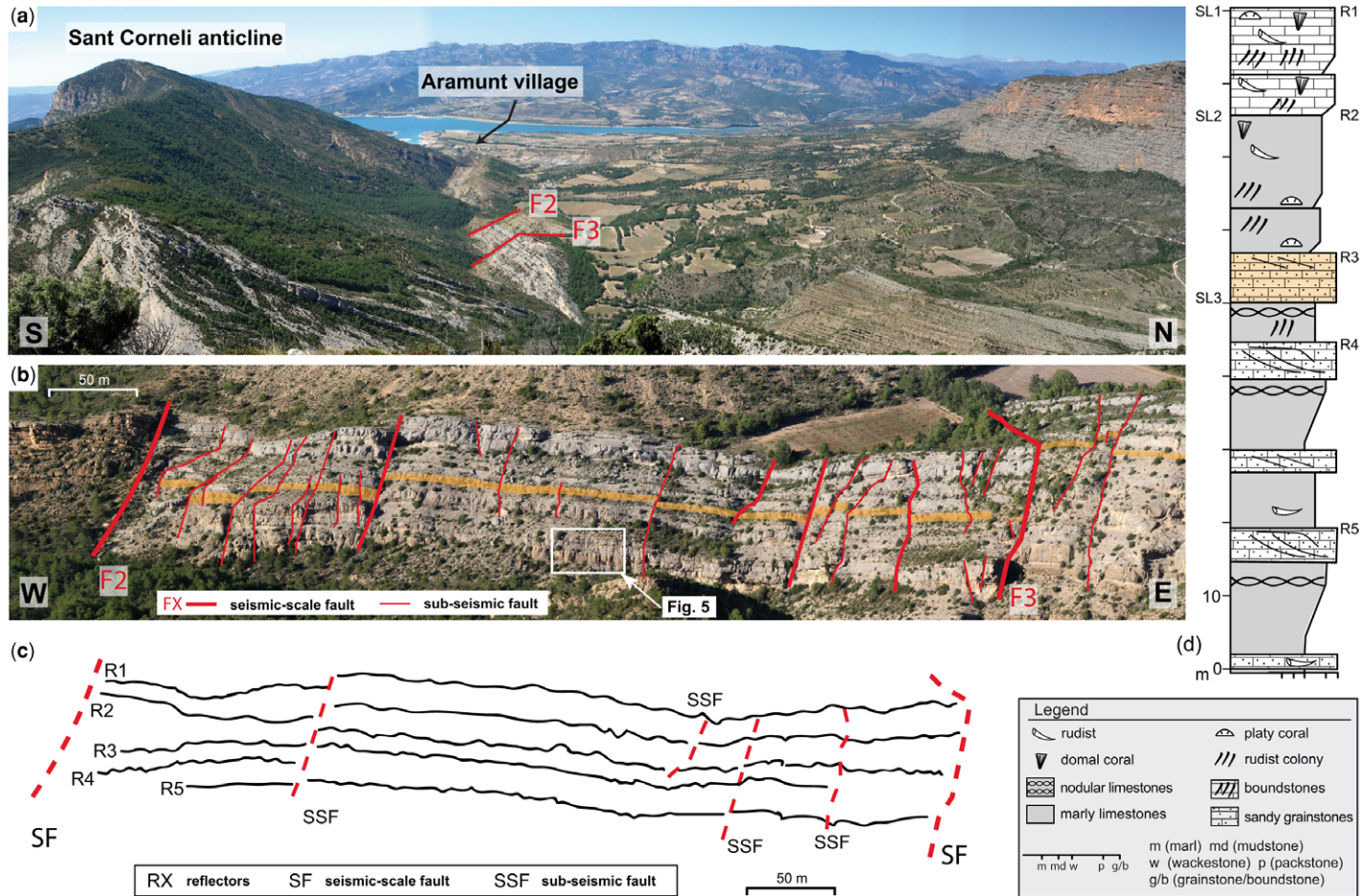
Fig. 4. (**a**) Panoramic view of the east–west-oriented Aramunt canyon in the northern limb of the Sant Corneli anticline and the seismic-scale faults F2 and F3 cross-cutting the canyon. (**b**) Panoramic view of the Aramunt outcrop looking north with seismic- to subseismic-scale faults sketched. (**c**) Idealized pseudo-seismic profile of the outcrop where the hypothetical main reflectors are indicated as R1 to R5. (**d**) Stratigraphic log. The brown layer is the uppermost sandy grainstone, reference level in (b).
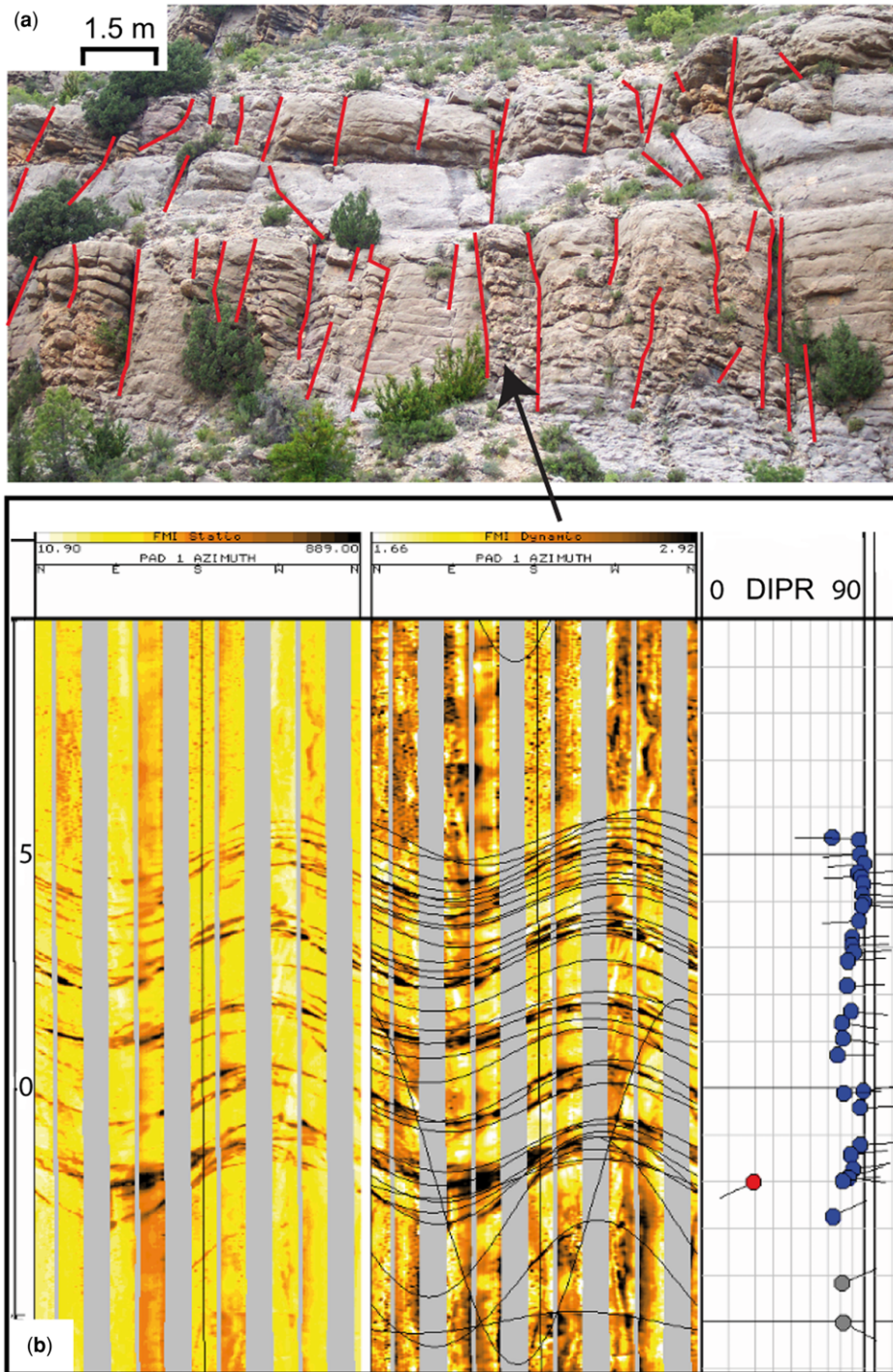
Fig. 5. Detail of the subseismic domain at the Aramunt outcrop. (**a**) Fractures cross-cut sandy grainstone and limestone layers. Note two types of fractures: stratabound and non-stratabound. Location in Figure 4b. (**b**) Example of a fracture corridor (*c.* 2 m wide) in a micro-resistivity image log from a highly deviated well in carbonates. The corridor is formed by a set of co-planar electrically conductive fractures striking north–south.

J. GUTMANIS *ET AL.*

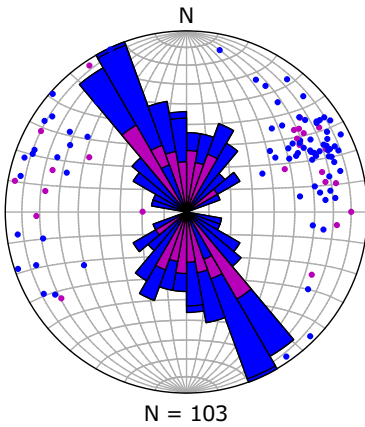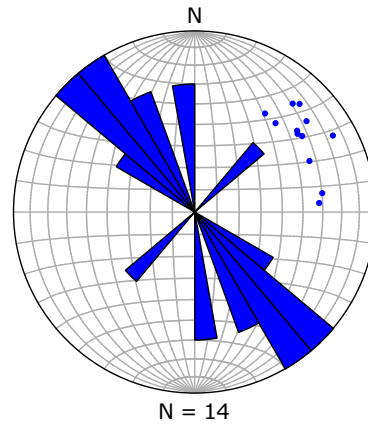SL 1 - upper rudist limestone

N

N = 267
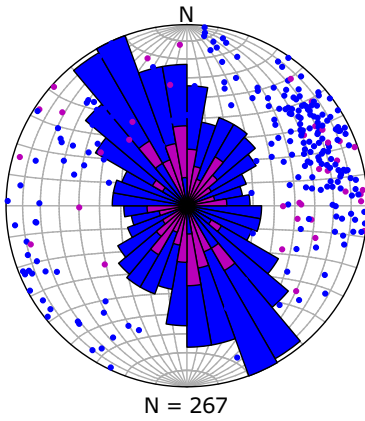
Legend

- faults
- fracture corridors
- background fractures
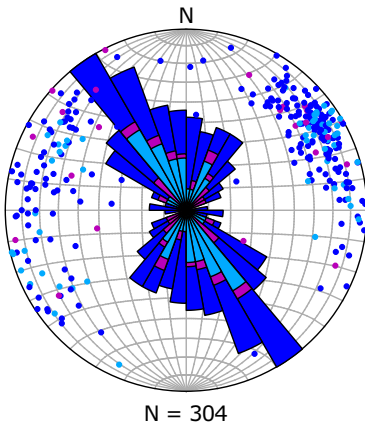
SL 1 - upper rudist limestone
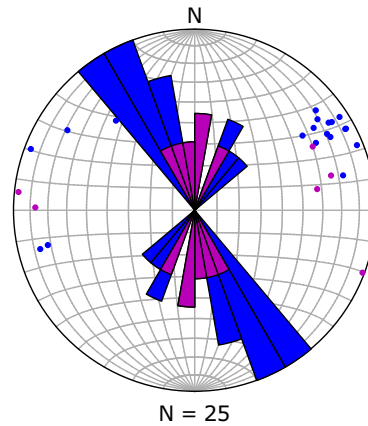(no outcrops)

SL 2 - lower rudist limestone

N

N = 103

SL 2 - lower rudist limestone

N

N = 14

SL 3 - sandy grainstone

N

N = 304

SL 3 - sandy grainstone

N

N = 25

fault F3

hanging wall

footwall

structures and directly imported into reservoir models as potential high-k (k: high permeability) pathways (e.g. Fonta *et al.* 2007; Souche *et al.* 2012).

The Aramunt data offer the opportunity to 'ground-truth' such a workflow. Average spacings of *c.* 150 m for SSF and *c.* 50 m for FC structures have a range that indicates clustering rather than regular spacings, commonly applied in static reservoir models. The spacing data can also help calibrate the interpretation of fracture clustering in borehole image logs, clustering which may be due either to the intersection of highly fractured mechanical units or to the intersection of fracture corridors (Fig. 5b). Distinguishing between these two different members of the fracture-scale hierarchy is important for fracture models as fracture corridors can have a large impact on reservoir connectivity. Unrealistically close (e.g. 10 m) SSF/FC spacings have sometimes been applied in static models.

Discussion

The Aramunt exposure provides useful insight into the typical nature, scale and distribution of fractures in the subseismic volume of a carbonate reservoir. It acts as a template for static fracture models by providing specific values for fracture attributes such as length, height, spacing and orientation, and their relationships with mechanical units. In addition, the parameters can help in the selection of appropriate grid cell sizes and domains for static and dynamic reservoir modelling. Domainal fracture models may be needed to distinguish, for example, the damage zones around faults F2 and F3 from the background fracture volume. Such domains might well deliver different results during hydraulic testing.

Hortoneda: Litho-mechanical control on stress and fracturing

The Hortoneda outcrop is a cliff forming the western side of a north–south-striking canyon north of Hortoneda village (the 'roca de Segués'). It reveals an axis-normal section through a Cretaceous structure interpreted as the western continuation of the Boumort anticline (Figs 1b & 8a). The stratigraphy consists of a thick section of marls and marly limestones of the Turonian Reguard Formation (Fig. 3), ending with three well-layered parasequences

(lower carbonate unit, Fig. 8a, c, d). Above is a poorly exposed marly interval which passes upward into the 75-m-thick upper carbonate unit referred to as the Congost Formation, mostly of Coniacian age. This consists of three lithofacies (Fig. 8a, b, d): a basal shoreface carbonate interval burrowed by *Thalasinoides*; an intermediate patch reef comprising two cycles of corals and rudists; and an upper grainstone with cross-bedding. Much of the lower two lithofacies are massive to thickly bedded and very nodular; the uppermost grainstone is more thinly bedded.

Both the upper and the lower carbonate units are folded within the Boumort antiform but they have different geometries and degrees of shortening, as discussed below. Both are heavily fractured but with markedly different types of fractures and fracture geometries, reflecting the mechanical properties of the lithologies and contrasting fold mechanisms.

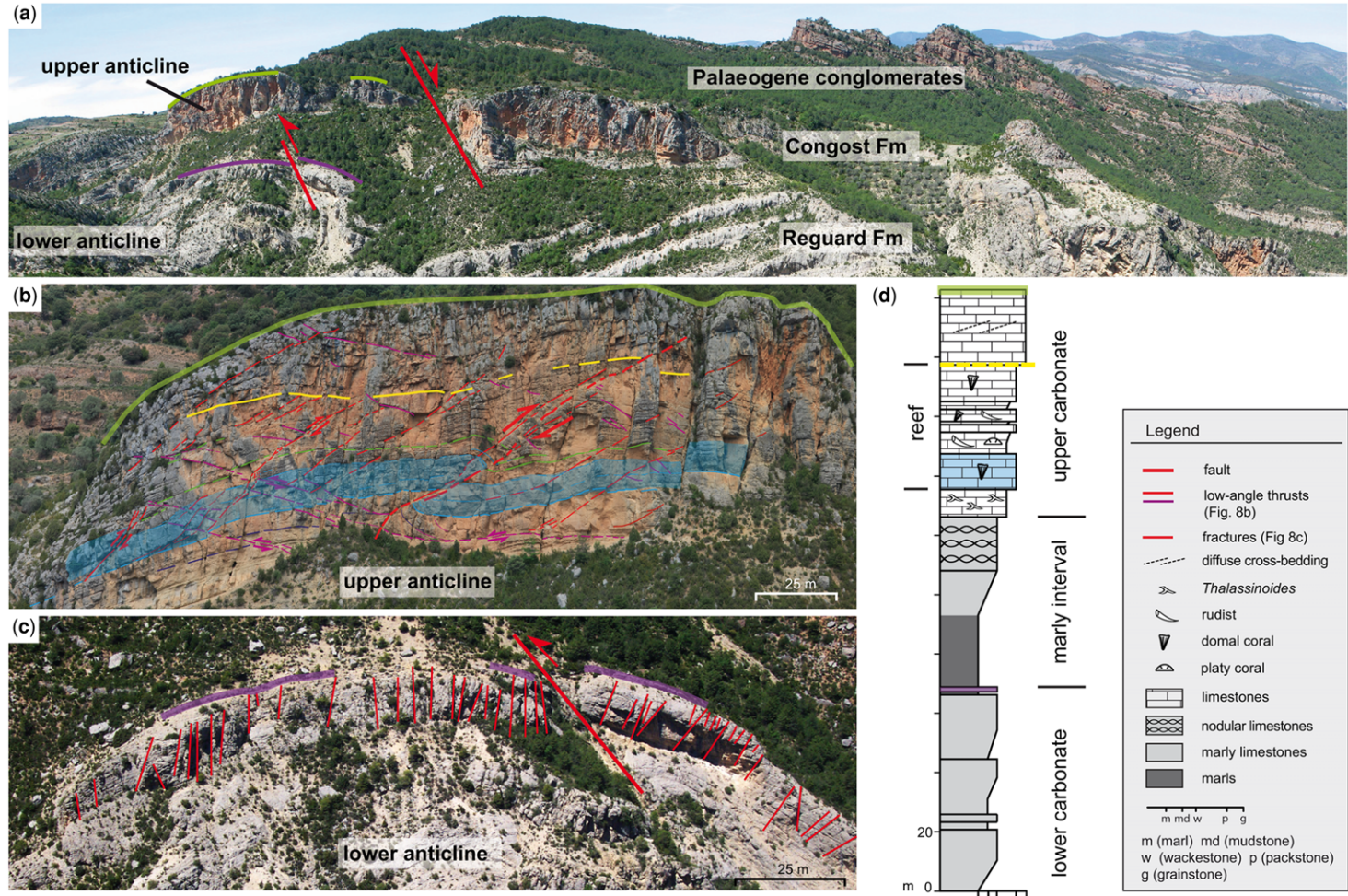### Fracturing in the upper carbonate unit

The earliest-formed fractures in the Coniacian upper limestone unit (Fig. 8b) are gently dipping, bed-parallel carbonate vein networks with bed-normal vertical growth fibres. These are cut by a system of opposed south- and north-directed low-angle thrusts, some of which sole out in bedding surfaces and contain ductile shear fabrics. A third family of fractures, the youngest, forms an extensive network of irregular, subvertical, brittle joints with axis-parallel, oblique and normal trends. Slickensides reveal both dip-slip and strike-slip movements on many of the joint surfaces, indicating minor fault displacement.

These geometries and relative timings imply that the Coniacian carbonate accommodated Pyrenean north–south compression by initial layer-parallel shortening and vertical uplift in conditions of high pore-fluid pressure (the bed-parallel vein system), followed by opposed thrusting and the development of a low-amplitude anticline. This style of deformation reflects the resistance to shortening (estimated at *c.* 8% from simple line length calculations) offered by the limestone, which is massive, nodular and generally competent. The younger, subvertical brittle joint system records extensional and transtensional strain and is interpreted from the orientation and kinematic data to be late- or post-tectonic.

Fig. 6. Stereonets showing strike orientation and poles to fracture and fault planes measured along three scan-lines (*c.* 500 m length) that were set up parallel to the bedding on top of the upper rudist limestone layer (SL1), on the base of the lower rudist limestone layer (SL2) and on the base of the sandy grainstone layer (SL3). Outcrop control points (GPS tracking and field waypoints) were taken along the scan-lines (*x*, *y*, *z* coordinates per 1 metre increment). See location of layers in the stratigraphic section (Fig. 4b, d). Fracture intensity along these scan-lines is shown in Figure 7a.
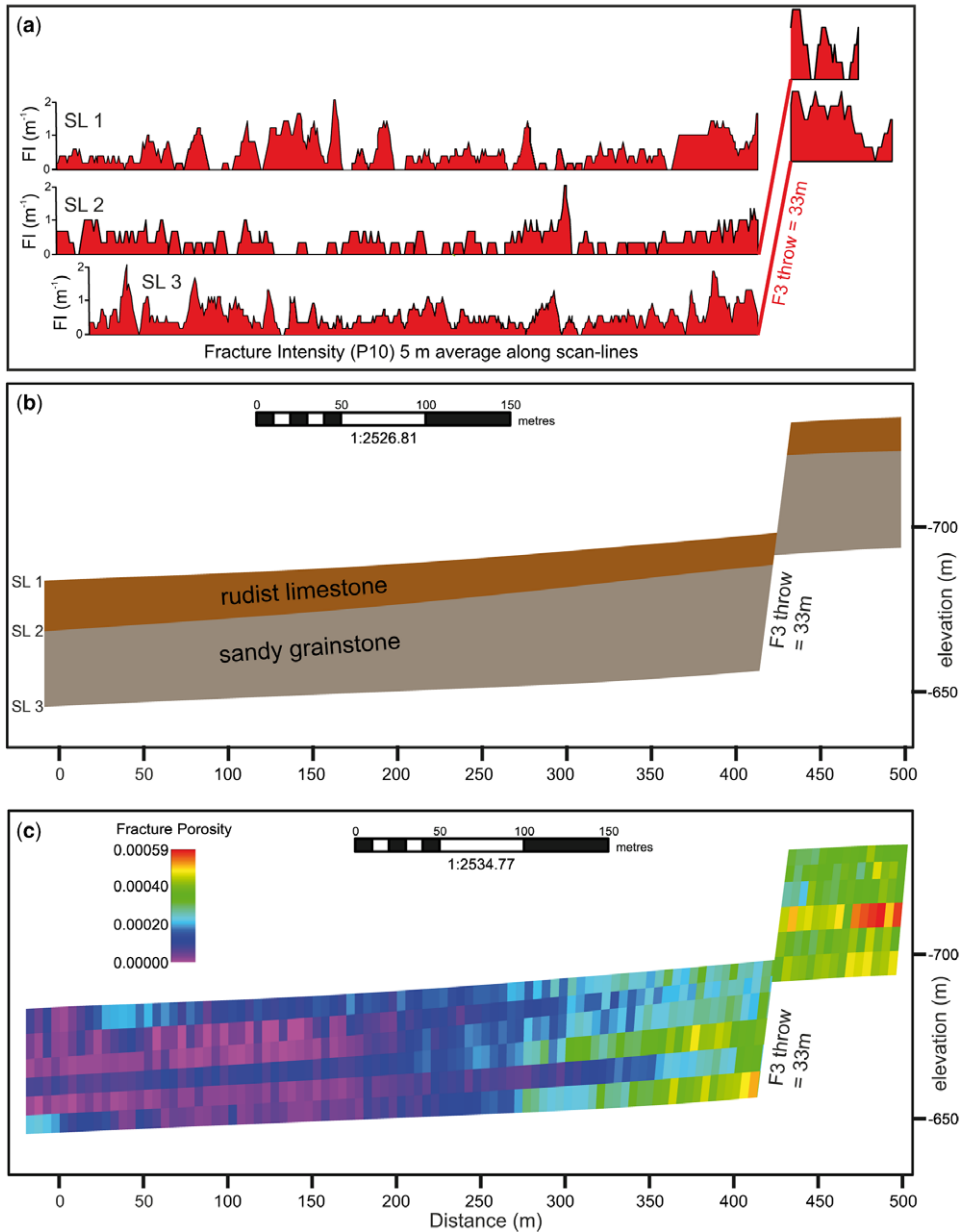
Fig. 7. Fracture porosity modelling of the Aramunt exposure in RMS software (Emerson Roxar). (**a**) Fracture intensity (P10) as a 5 m rolling average along scan-lines SL1 to SL3, which were treated as synthetic wells (see location on Fig. 6). The synthetic wells were established by importing GPS coordinates, heads and well trajectories into the software. Fracture dip, dip azimuth, type and intensity were then imported into the synthetic wells. (**b**) Cross-section of the reservoir zonation showing the rudist limestone and grainstone zones and fault F3. The stratigraphic units were based on GPS coordinates, elevation and bedding parameters. The F3 fault was modelled deterministically using displacements measured in the field, and a geomodel grid created for the faults and horizons using pillar fault modelling. Subseismic faults and fracture corridors were modelled stochastically using a discrete fracture network (DFN) model conditioned to the field data. (**c**) Cross-section of the fracture porosity model built from the scaled-up discrete fracture network model and conditioned to fracture apertures (200 μm for seismic-scale faults, 100 μm for fracture corridors and 25 μm for background fractures). These values were selected from a review of analogue data acquired in subsurface reservoir characterization studies in similar geological settings.

Fig. 8. (**a**) Panoramic view of the Hortoneda outcrop with major faults and anticlines indicated. (**b**) Fracture pattern in the upper massive carbonate unit. (**c**) Fracture pattern in the lower, well-layered carbonate unit. (**d**) Stratigraphic log. See green, yellow, blue and purple layers as reference levels.

It may record residual stress release during exhumation, since immediately above the Hortoneda cliff exposure there is a Late Eocene exhumation surface re-exposed by the current topography.

Fracturing in the lower carbonate unit

A system of mainly bed-orthogonal extensional and locally conjugate shear fractures is developed in the lower carbonate unit (Fig. 8c). It forms a generally quasi-radial axial fracture pattern, complicated locally by the presence of faults and their damage zones. The fracture orientations are similar to those in the upper limestone unit; oblique trends are less well developed. There is no evidence of bed-parallel fracturing or low-angle thrusting, although steep reverse faults accommodate some shortening on the northern limb.

In contrast to the massive upper limestone unit, the well-layered Turonian carbonates responded to the north–south compression with a more classical fold mechanism associated with outer arc extension and, on the limbs, bed-parallel flexural slip. The shortening is estimated at *c.* 15% and the anticline is markedly tighter. The difference in shortening between the anticlines in the upper and lower units was accommodated by the intervening marly interval, which probably acted as a décollement. Although exposure is poor, small-scale folds in the marls imply shortening and local thickening.

Discussion

The geometry of the two Hortoneda anticlines and their associated fracture patterns 'fossilize' the stress caused by the contrasting litho-mechanical
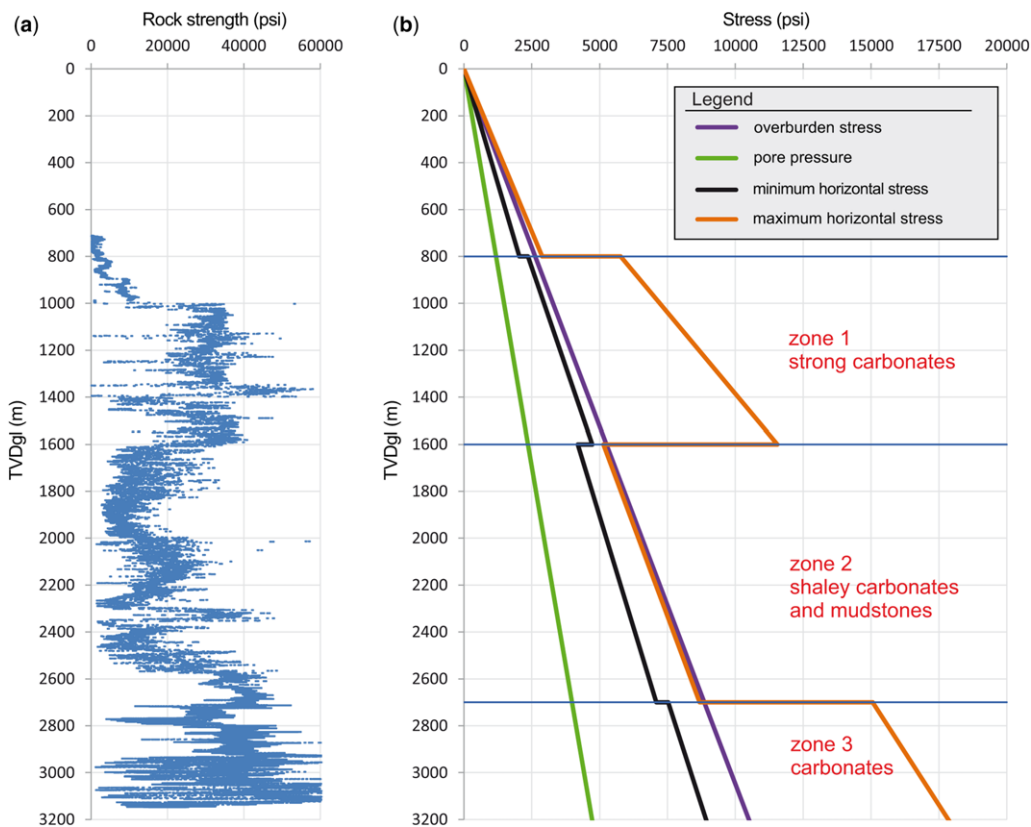
Fig. 9. Data from an exploration well in a highly layered carbonate/shale/mudstone sequence in an active fold-and-thrust belt. (**a**) Rock strength profile built from sonic and density logs using the Coates–Denoo equation (Coates & Denoo 1981). (**b**) *In situ* stress profile built using methodology described in the text and showing three geomechanical zones closely tied to rock strength. Zones 1 and 3 are high-strength carbonate-dominated intervals with strike-slip and relatively high-differential stress. Zone 2 is dominated by relatively weak shaly carbonates and mudstones and is associated with a low-differential, normal stress condition. Image log fracture intensities are higher in zones 1 and 3 than in zone 2.

properties of the formations (rock strength, elastic *moduli* and degree of layer anisotropy). To illustrate, we compare Hortoneda with an example of an *in situ* stress profile that can be seen in a still active fold-and-thrust belt of the Middle East (Fig. 9). The profile is from a deep exploration well at the crest of a fault-propagation fold. The well penetrates 4 km of Tertiary–Upper Triassic carbonates, some massive and some layered, interrupted by relatively weak marls and shales, thin carbonate interbeds and evaporites (mainly anhydrite).

The *in situ* stress profile was constructed as follows:

(a) integration of density logs from the surface to derive overburden stress magnitude with depth (S_v);
(b) processing of sonic and density logs to estimate rock strength with depth, calibrated with core testing data for unconfined uniaxial strength;
(c) estimation of minimum horizontal stress magnitude (S_{Hmin}) with tectonic strain, calibrated to leak off test data; and
(d) estimation of maximum horizontal stress (S_{Hmax}) by calibration to S_v and S_{Hmin} together with observations of wellbore failure (breakout, induced axial fracturing).

A close coupling between rock strength, differential stress magnitude and stress regime (normal or strike slip) is illustrated in Figure 9. The 800–1600 m depth interval is formed mainly by strong Upper Cretaceous carbonates which are able to sustain a high differential, strike-slip stress condition. By contrast, the Lower Cretaceous–Upper Jurassic interval from 1600 to *c.* 2700 m is dominated by weaker, often more ductile rocks associated with lower differential stress and a normal stress condition. At greater depth, high differential strike-slip stress is seen again in Jurassic and Triassic formations. A further observation in the well profile is that fracture intensity is closely coupled to the changes of *in situ* stress and rock properties. High intensities of brittle fractures are seen in the rocks that are capable of bearing greater differential stress, while lower intensities are seen in the weaker, more ductile lithologies.

The stress profile is typical of an active structure with relatively high stress anisotropy (a 'stress-sensitive' structure in the terminology of Smart *et al.* 2001). We suggest that the stress state that developed through the Hortoneda section during contractional deformation was similarly due to the variations of litho-mechanical properties with depth.

The Hortoneda outcrop also illustrates the difficulties associated with the use of seismic-based curvature analysis to predict fracture intensity distribution across folds. It is often assumed that a high rate of curvature in a seismically mapped surface

can be a proxy for high fracture intensity (e.g. Lisle 1995; Roberts 2001). The issue is contentious; see, for example, the review by Bergbauer (2007). Curvature analysis may be reasonably valid for folds formed by the tangential longitudinal shear mechanism where outer arc extension takes place, and therefore higher fracture intensity is predicted at the crest (Ramsay 1967; Hudleston & Treagus 2010). However, highly layered sequences with contrasting mechanical properties such as those discussed here are more likely to deform by the flexural slip mechanism in which strains are concentrated on the limbs rather than the crest, or with a combination of tangential longitudinal shear, flexural slip and flexural flow (Cosgrove & Ameen 2000; Hudleston & Treagus 2010). Each litho-mechanical unit may therefore have a subtly different fracture character due to the interplay between rock strength, layer boundary strength, layer anisotropy, fold mechanism and deformation depth (Bazalgette & Petit 2007). The use of curvature analysis should be constrained by an evaluation of the litho-mechanical profile and likely fold mechanism of the structure in question, built from wireline log and core test data.

Bóixols: characterizing fault damage zones

The Bóixols outcrop is a road cutting located along road C-363, 1.5 km east of Bóixols village (Figs 1, 2 & 10a). A well-exposed thrust plane dipping 25°N contains pressure-solution cleavage and slip planes whose geometry indicates top-to-the-south movement. By analogy with similar structures in the region (e.g. Lacroix *et al.* 2011) the structure probably formed at significant depth, around 5 km. It has caused a relatively small (*c.* 30 m) offset of a stratigraphically reduced Upper Cretaceous section in the steeply south-dipping forelimb of the Bóixols anticline, and is therefore interpreted as a local accommodation structure or perhaps a hanging-wall splay of the main Bóixols thrust. In the immediate footwall of the fault slightly overturned, massive to well-bedded limestones and sandy grainstones occur that were deposited in a condensed and shallow shelf setting, mostly during Coniacian time (Fig. 3). The evolution of a complex fracture system is related to propagation of the fault plane.

Fracturing in the footwall damage zone

The fracture types present in the footwall damage zone are, from oldest to youngest, indicated by offsetting relationships (Fig. 10b):

(a) bed-parallel stylolites which originated normal to the overburden stress (S_v) during burial and were later reactivated (see (d) below);
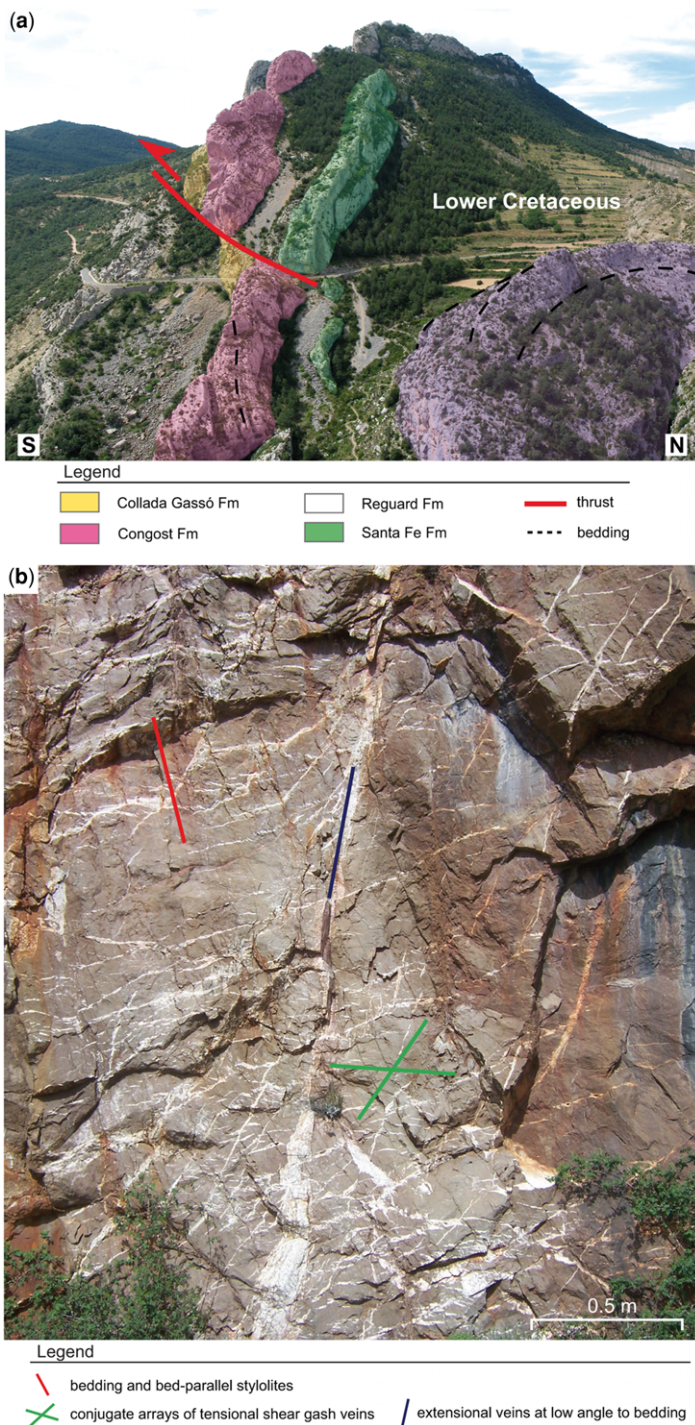
Fig. 10. (**a**) Panoramic view of the southern limb of the Bóixols anticline, showing vertical to overturned Upper Cretaceous strata (Santa Fe to Collada Gassó lithostratigraphic units) (Figs 2 & 3). The Bóixols outcrop is located along the roadside, in the footwall of the thrust. (**b**) Detail of the footwall damage zone of the Bóixols outcrop in the Collada Gassó Formation.

(b) sets of large veins oriented at low angle to bedding with composite crack-seal calcite fills (Bons *et al.* 2012), implying episodic extension in a direction oblique to the bedding and probably associated with early fold growth and limb tilt;

(c) conjugate vein arrays of calcite-filled tension gashes whose bisector implies a subhorizontal maximum stress (S_{Hmax}), interpreted as a record of the maximum shortening phase;

(d) stylolite reactivation causing offsets of (c), also associated with maximum shortening; and

(e) late brittle fractures indicating dip-slip to strike-slip movement, interpreted as late- to post-tectonic relaxation.

The stylolites, extensional veins and conjugate vein arrays are numerous and highly localized in the footwall of the fault, forming a damage zone, but become rare some 50–100 m below the thrust. In general, they do not occur in the hanging wall except where a minor secondary splay fault appears to intersect the main fault downdip to the north. The late brittle fractures are more pervasively distributed.

In summary, the Bóixols outcrop is interpreted as a good example of a 'fossilized' fault damage zone. The fracture system has been well preserved by the high percentage of calcite fills. Subsequent brittle fracturing imposed some younger porosity, but the footwall damage zone is essentially a zone of low fracture porosity and permeability.

Discussion

The Bóixols reverse fault is a splay thrust which breaches the steeply dipping to overturned southern limb of the Bóixols anticline and cuts Upper Cretaceous strata. We interpret the fracture pattern in the footwall damage zone as a record of transient fracturing with relatively rapid 'self-sealing' by precipitation of calcite fills. The fracturing was initiated by short-term trapping of pore fluids in a dilational zone below the propagating fault plane. This mechanism of transient fracturing has been described as pressure release by 'fault-valving' (e.g. Sibson 2004) and been described in other geological settings, for example during burial of mudrocks in an extensional basin (Cosgrove 2001) and in association with episodic fault rupture and propagation during the seismic cycle (Woodcock *et al.* 2007). For this interpretation to hold true, the Bóixols thrust fault plane must have acted as a transient low-permeability sealing structure at this locality, suggesting that it was in a relatively low-stress, dormant stage of the seismic cycle at that time. A similar structural history and associated damage zone has been described in footwall outcrops of the Absaroka Thrust in the USA (Wiltschko *et al.* 2009).

Many outcrop studies have shown that fault zones usually consist of a central zone of fault rock, representing the fault rupture planes, surrounded by other zones of high strain termed 'damage zones' (e.g. Caine *et al.* 1996; Childs *et al.* 2009; Faulkner *et al.* 2010). The latter contain enhanced fracture intensity at both matrix-scale (grain-scale micro-fracturing) and meso-scale. Fault rocks typically have reduced porosity and permeability due to cataclasis and thermo-chemical alteration of the hostrock during fault propagation, whereas the adjacent damage zones tend to be relatively permeable volumes with open and connected fractures. In fact, damage zones are often a prime target for exploration or development wells.

The Bóixols outcrop is a good example of the opposite case, in which the damage zone would be largely characterized as poor-quality reservoir because any porosity created during fracturing was largely destroyed by the self-sealing process. Similar zones can be inferred in hydrocarbon wells where clusters of sealed fractures occur adjacent to fault planes that are associated with pressure boundaries. Two factors could potentially counter this negative scenario. Firstly, the damage zone could have become charged with hydrocarbon prior to the self-sealing process, in which case some reservoir potential could still be preserved. Faults are believed to be important routes for hydrocarbon migration during their active phases (e.g. Muir-Wood 1994; Moretti 1998). Secondly, new fracture porosity may be created during a subsequent tectonic phase at shallower depth and in the absence of mineral precipitation from formation or hydrothermal fluids, or during exhumation and dissolution. The timing of these porosity-creating and porosity-occluding processes relative to hydrocarbon migration and charging is crucial.

The Bóixols outcrop therefore provides a useful analogue for image log interpretation in hydrocarbon wells. It also indicates that good storage or production properties cannot be assumed for fault damage zones in advance of drilling and testing, and that an evaluation of hydrocarbon migration history, fault activity history, the current *in situ* stress regime and analogue properties should be part of a workflow aimed at identifying the subset of faults with the best potential.

Conclusions

The fractured carbonate outcrops described here all provide useful analogue observations, data and concepts to support subsurface hydrocarbon reservoir characterization from well and seismic data. Aramunt provides insights into the scale and distribution of fractures in the subseismic volume;

Hortoneda illustrates the coupled behaviour between active stress and litho-mechanical properties at the time of fracture development; and Bóixols provides information about fracture evolution and distribution in fault damage zones, especially the delicate balance between porosity-creating processes and porosity-occluding processes.

Given that much subsurface data interpretation involves a relatively high degree of subjectivity and expert judgement, we suggest that analogues such as these (and many others around the world) are at the very least useful and, at best, essential to the success of the process. Many routine methods for reservoir evaluation in 1D datasets such as the logging of core, interpretation of borehole image logs or full waveform sonic data, and the interpretation of *in situ* stress and pore fluid profiles could be enhanced and calibrated by the application of analogues such as those described here.

Fracture parameters which are difficult or impossible to quantify in subsurface data, especially length and height (aspect ratio), connectivity and relationship to mechanical units, spacings and dimensions of meso-scale structures (fracture corridors) can all be evaluated at the outcrops. In addition, the analogues can be applied in the workflow for building and verifying reservoir models, and in 'ground-truthing' the outputs from software and seismic analysis techniques that generate interpretations from limited input data. Analogue information can be useful in many contexts beyond fractured carbonate hydrocarbon reservoirs, for example fractured clastic or basement reservoirs and, potentially, geothermal reservoirs or carbon storage projects, wherever it is necessary to understand how the fracture system influences performance.

References

ARTHUR, J.M., LAWTON, D.C. & WONG, J. 2015. Physical modeling of a near-vertical fault zone. *Search and Discovery*, Article #41515.

AYDIN, A., ANTONELLINI, M., TONDI, E. & AGOSTA, F. 2010. Deformation along the leading edge of the Maiella thrust sheet in central Italy. *Journal of Structural Geology*, **32**, 1291–1304.

BAZALGETTE, L. & PETIT, J.P. 2007. Fold amplification and style transition involving fractured dip-domain boundaries: buckling experiments in brittle paraffin wax multilayers and comparison with natural examples. *In*: LONERGAN, L., JOLLY, R.J.H., RAWNSLEY, K. & SANDERSON, D.J. (eds) *Fractured Reservoirs*. Geological Society, London, Special Publications, **270**, 157–169, https://doi.org/10.1144/GSL.SP.2007.270.01.11

BELAYNEH, M., MATTHAI, S.K. & COSGROVE, J.W. 2007. The implications of fracture swarms in the Chalk of SE England on the tectonic history of the basin and their impact on fluid flow in high-porosity, low-permeability rocks. *In*: RIES, A.C., BUTLER, R.W.H. & GRAHAM, R.H. (eds) *Deformation of the Continental Crust: The Legacy of Mike Coward*. Geological Society, London, Special Publications, **272**, 499–517, https://doi.org/10.1144/GSL.SP.2007.272.01.25

BERÁSTEGUI, X., SENZ, J.G. & LOSANTOS, M. 1990. Tectosedimentary evolution of the Organyà extensional basin (Central South-Pyrenean Unit, Spain) during the Lower Cretaceous. *Bulletin de la Société Géologique de France*, **8**, 251–264.

BERGBAUER, S. 2007. Testing the predictive capability of curvature analysis. *In*: JOLLEY, S.J., BARR, D., WALSH, J.J. & KNIPE, R.J. (eds) *Structurally Complex Reservoirs*. Geological Society, London, Special Publications, **292**, 185–202, https://doi.org/10.1144/SP292.11

BOND, R.M.G. & McCLAY, K.R. 1995. Inversion of a Lower Cretaceous extensional basin, south-central Pyrenees, Spain. *In*: BUCHANAN, J.G. & BUCHANAN, P.G. (eds) *Basin inversion*. Geological Society, London, Special Publication, **88**, 415–431, https://doi.org/10.1144/GSL.SP.1995.088.01.22

BONS, P.D., ELBURG, M.A. & GÓMEZ-RIVAS, E. 2012. A review of the formation of tectonic veins and their microstructures. *Journal of Structural Geology*, **43**, 33–62.

CAINE, J.S., EVANS, J.P. & FORSTER, C.B. 1996. Fault zone architecture and permeability structure. *Geology*, **24**, 1025–1028.

CASINI, G., GILLESPIE, P.A. *ET AL.* 2011. Sub-seismic fractures in foreland fold and thrust belts: insight from the Lurestan Province, Zagros Mountains, Iran. *Petroleum Geoscience*, **17**, 263–282, https://doi.org/10.1144/1354-079310-043

CHILDS, C., MANZOCCHI, T., WALSH, J.J., BONSON, C.G., NICOL, A. & SCHOPFER, M. 2009. A geometric model of fault zone and fault rock thickness variations. *Journal of Structural Geology*, **31**, 117–127.

CHOUKROUNE, P. & ECORS PYRENEES TEAM 1989. The ECORS Pyrenean deep seismic profile reflection data and the overall structure of an orogenic belt. *Tectonics*, **8**, 23–39.

COATES, G.R. & DENOO, S.A. 1981. Mechanical properties program using borehole analysis and Mohrs circle. *SPWLA 22nd Annual Logging Symposium*, 23–26 June, Mexico.

COOKE, M.L. & UNDERWOOD, C.A. 2001. Fracture termination and step-over at bedding interfaces due to frictional slip and interface opening. *Journal of Structural Geology*, **23**, 223–238.

COSGROVE, J.W. 2001. Hydraulic fracturing during the formation and deformation of a basin: A factor in the dewatering of low-permeability systems. *AAPG Bulletin*, **85**, 737–748.

COSGROVE, J.W. & AMEEN, M.S. 2000. A comparison of the geometry, spatial organisation and fracture patterns associated with forced folds and buckle folds. *In*: COSGROVE, J.W. & AMEEN, M.S. (eds) *Forced Folds and Fractures*. Geological Society, London, Special Publications, **169**, 7–21, https://doi.org/10.1144/GSL.SP.2000.169.01.02

COUPLES, G.D., LEWIS, H. & TANNER, G. 1998. Strain partitioning during flexural slip folding. *In*: COWARD, M.P., DALTABAN, M.P. & JOHNSON, H. (eds) *Structural Geology in Reservoir Characterisation*. Geological Society, London, Special Publications, **127**, 149–165, https://doi.org/10.1144/GSL.SP.1998.127.01.12

FAULKNER, D.R., JACKSON, C.A.L., LUNN, R.J., SCHLISCHE, R.W., SHIPTON, Z.K., WIBBERLEY, C.A.J. & WITHJACK, M.O. 2010. A review of recent devlopments concerning the structure, mechanics and fluid flow properties of fault zones. *Journal of Structural Geology*, **32**, 1557–1575.

FONTA, O., AL-AJMI, H., VERMA, N.K., MATAR, S., DIVRY, V. & AL-QALLAF, H. 2007. The fracture characterisation and fracture modeling of a tight carbonate reservoir – the Najmah-Sargelu of West Kuwait. *SPE Reservoir Evaluation & Engineering*, **10**, 93577.

GALLEMÍ, J., MARTÍNEZ, R. & PONS, J.P. 1982. Unidades del Cretácico superior en los alrededores de Sant Corneli (Província de Lleida). *Cuadernos de Geología Ibérica*, **8**, 935–948.

GARCIA-SENZ, J. 2002. *Cuencas extensivas del Cretácico Inferior en los Pirineos centrales, formación y subsecuente inversión*. PhD thesis, Departament de Geodinàmica i Geofísica, Universitat de Barcelona.

GOUTH, F., TOUBLANC, A. & MRESAH, M. 2006. Characterisation and modeling of a fractured reservoir using a novel DFN approach. In *Proceedings of Abu Dhabi International Petroleum Exhibition and Conference*, Abu Dhabi, UAE, SPE 10216.

HUDLESTON, P.J. & TREAGUS, S.H. 2010. Information from folds: a review. *Journal of Structural Geology*, **32**, 2042–2071.

KLIMCZAK, C., SCHULTZ, R.A., PARASHAR, R. & REEVES, D.M. 2010. Cubic law with aperture-length correlation: implications for network scale fluid flow. *Hydrogeology Journal*, **18**, 851–862.

LACROIX, B., BAUTIER, M. ET AL. 2011. Microtectonic and geochemical characterisation of thrusting in a foreland basin: example of the south-Pyrenean orogenic wedge (Spain). *Journal of Structural Geology*, **33**, 1359–1377.

LAUBACH, S.E., OLSON, J.E. & GROSS, M.R. 2009. Mechanical and fracture stratigraphy. *AAPG bulletin*, **93**, 1413–1426.

LISLE, R.J. 1995. The Mohr circle for curvature and its application to fold description. *Journal of Structural Geology*, **17**, 739–750.

MENCOS, J., MUÑOZ, J.A. & HARDY, S. 2011. Three-dimensional geometry and forward numerical modeling of the Sant Corneli anticline (southern Pyrenees, Spain). *In*: MCCLAY, K.R. (ed.) *Thrust Fault-Related Folding*, AAPG, Boulder, Memoir **94**, 283–300.

MENCOS, J., CARRERA, N. & MUÑOZ, J.A. 2015. Influence of rift basin geometry on the subsequent postrift sedimentation and basin inversion: the Organyà basin and the Bóixols thrust sheet (South-Central Pyrenees). *Tectonics*, **34**, 1452–1474.

MEY, P.H.V., NAGTEGAAL, P.J.C., ROBERTI, K.J. & HARTEVELT, J.J.A. 1968. Lithostratigraphic subdivision of post-Hercynian deposits in the south-central Pyrenees, Spain. *Leidse Geologische Mededelingen*, **41**, 221–228.

MORETTI, I. 1998. The role of faults in hydrocarbon migration. *Petroleum Geoscience*, **4**, 81–94, https://doi.org/10.1144/petgeo.4.1.81

MUIR-WOOD, R. 1994. Earthquakes, strain-cycling and the mobilisation of fluids. *In*: PARNELL, J. (ed.) *Geofluids: Origin Migration and Evolution of Fluids in Sedimentary Basins*. Geological Society, London, Special Publications, **78**, 85–98, https://doi.org/10.1144/GSL.SP.1994.078.01.08

MUÑOZ, J.A. 1992. Evolution of a continental collision belt: ECORS-Pyrenees crustal balanced cross-section. *In*: MCCLAY, K.R. (ed.) *Thrust Tectonics*. Chapman and Hall, London, 235–246.

MUÑOZ, J.A., CARRERA, N. ET AL. 2010. *Cartografia geològica del substrat prequaternari Aramunt 1:25000*. Institut Cartogràfic i Geològic de Catalunya (ICGC), Barcelona, 252–2–2 (66–22).

NARR, W., SCHECTER, D.W. & THOMPSON, L.B. 2006. *Naturally Fractured Reservoir Characterisation*. Society of Petroleum Engineers, Richardson, TX.

NELSON, R.A. 2001. *Geologic Analysis of Naturally Fractured Reservoirs*. 2nd edn. Gulf Professional Publishing, Butterworth-Heinemann, Boston.

NELSON, R.A., MOLDOVANYI, E.P., MATCEK, C.C., AZPIRITXAGA, I. & BUENO, E. 2000. Production characteristics of the fractured reservoirs of the La Paz field, Maracaibo Basin, Venezuela. *AAPG Bulletin*, **84**, 1791–1809.

OGATA, K., SENGER, K., BRAATHEN, A. & TVERANGER, J. 2014. Fracture corridors as seal-bypass systems in siliciclastic reservoir cap-rock successions: field-based insights from the Jurassic Entrada Formation (SE Utah, USA). *Journal of Structural Geology*, **66**, 162–187.

POMAR, L., GILI, E., OBRADOR, A. & WARD, W.C. 2005. Facies architecture and high-resolution sequence stratigraphy of an Upper Cretaceous platform margin succession, southern central Pyrenees, Spain. *Sedimentary Geology*, **175**, 339–365.

PUIGDEFÀBREGAS, C. & SOUQUET, P. 1986. Tecto-sedimentary cycles and depositional sequences of the Mesozoic and Tertiary from the Pyrenees. *Tectonophysics*, **129**, 173–203.

RAMSAY, J.G. 1967. *Folding and Fracturing of Rocks*. McGraw Hill, New York.

ROBERTS, A. 2001. Curvature attributes and their application to 3D interpreted horizons. *First Break*, **19**, 85–99.

SASSI, W., GUITON, M.L.E., LEROY, Y.M., DANIEL, J.M. & CALLOT, J.P. 2012. Constraints on bed scale fracture chronology with a FEM mechanical model of folding: The case of Split Mountain (Utah, USA). *Tectonophysics*, **576**, 197–215.

SÉGURET, M. 1972. *Etude tectonique des nappes et séries décollées de la partie centrale du versant sud des*

Pyrénées: Caractere synsédimentaire, rôle de la compression et de la gravité. Publications de l'Université des Sciences et Techniques du Languedoc (USTELA), Série Géologie Structurale, 2.

SHACKLETON, J.R., COOKE, M.L. & SUSSMAN, A.J. 2005. Evidence for temporally changing mechanical stratigraphy and effects on joint-network architecture. *Geology*, **33**, 101–104.

SHACKLETON, J.R., COOKE, M.L., VERGÉS, J. & SIMÓ, T. 2011. Temporal constraints on fracturing associated with fault-related folding at Sant Corneli anticline, Spanish Pyrenees. *Journal of Structural Geology*, **33**, 5–19.

SIBSON, R.H. 2004. Frictional mechanics of seismogenic thrust systems in the upper continental crust – implications for the fluid overpressures and redistribution. *In*: MCCLAY, K.R. (ed.) *Thrust Tectonics and Hydrocarbon Systems*. AAPG, Boulder, Memoir **82**, 1–17.

SINGH, S.K., ABU-HABBIEL, H., KHAN, B., AKBAR, M., ETCHECOPAR, A. & MONTARON, B. 2008. Mapping fracture corridors in naturally fractured reservoirs: an example from Middle East carbonates. *First Break*, **26**, 109–113.

SKELTON, P.W., GILI, E., VICENS, E., OBRADOR, A. & LÓPEZ, G. 2003. Revised lithostratigraphy of the Upper Cretaceous (Santonian) carbonate platform succession on the northern flank of Sant Corneli, southern Central Pyrenees. *Journal of Iberian Geology*, **29**, 73–87.

SMART, B.G.D., SOMERVILLE, J.M., EDLMAN, K. & JONES, C. 2001. Stress sensitivity of fractured reservoirs. *Journal of Petroleum Science and Engineering*, **29**, 29–37.

SOUCHE, L., ASTRATTI, D., AARRE, V., CLERC, N., CLARK, A., AL DAYYNI, T.N.A. & MAHMOUD, S.L. 2012. A dual representation of multiscale fracture network modelling: application to a giant UAE carbonate field. *First Break*, **30**, 43–52.

STEPHENSON, B.J., KOOPMAN, A., HILLGARTNER, H., MCQUILLAN, H., BOURNE, S., NOAD, J.J. & RAWNSLEY, K. 2007. Structural and stratigraphic controls on fold-related fracturing in the Zagros Mountains, Iran: implications for reservoir development. *In*: LONERGAN, L., JOLLY, R.J.H., RAWNSLEY, K. & SANDERSON, D.J. (eds) *Fractured Reservoirs*. Geological Society, London, Special Publications, **270**, 1–21, https://doi.org/10.1144/GSL.SP.2007.270.01.01

TAVANI, S., MENCOS, J., BAUSA, J.A. & MUÑOZ, J.A. 2011. The fracture pattern of the Sant Corneli Bóixols oblique inversion anticline (Spanish Pyrenees). *Journal of Structural Geology*, **33**, 1662–1680.

TAVANI, S., STORTI, F., LACOMBE, O., CORRADETI, A., MUÑOZ, J.A. & MAZZOLI, S. 2015. A review of deformation pattern templates in foreland basin systems and fold and thrust belts: implications for the state of stress in the frontal regions of thrust wedges. *Earth-Science Reviews*, **141**, 82–104.

VERGÉS, J. & MUÑOZ, J.A. 1990. Thrust sequences in the southern central Pyrenees. *Bulletin de la Société Géologique de France*, **8**, 265–271.

VICENS, E., LÓPEZ, G. & OBRADOR, A. 1998. Facies succession, biostratigraphy and rudist faunas of Coniacian to Santonian platform deposits in the Sant Corneli anticline (South Central Pyrenees). *Geobios*, **22**, 403–427.

WELCH, M.J., SOUQUE, C., DAVIES, R.K. & KNIPE, R.J. 2015. Using mechanical models to investigate the controls on fracture geometry and distribution in chalk. *In*: AGAR, S.M. & GEIGER, S. (eds) *Fundamental Controls on Fluid Flow in Carbonates: Current Workflows to Emerging Technologies*. Geological Society, London, Special Publications, **406**, 281–309, https://doi.org/10.1144/SP406.5

WENNBERG, O.P., SVÅNÅ, T., AZIZZADEH, M., AQRAWI, A.M.M., BROCKBANK, P., LYSLO, K.B. & OGILVIE, S. 2006. Fracture intensity v. mechanical stratigraphy in platform top carbonates: The Aquitanian of the Asmari Formation, Khaviz Anticline, Zagros, SW Iran. *Petroleum Geoscience*, **12**, 235–246, https://doi.org/10.1144/1354-079305-675

WILTSCHKO, D.V., LAMBERT, G.R. & LAMB, W. 2009. Conditions during syntectonic vein formation in the footwall of the Absaroka Thrust Fault, Idaho-Wyoming-Utah fold and thrust belt. *Journal of Structural Geology*, **31**, 1039–1057.

WOODCOCK, N.H., DICKSON, J.A.D. & TARASEWICZ, J.P.T. 2007. Transient permeability and reseal hardening in fault zones: evidence from dilation breccia textures. *In*: LONERGAN, L., JOLLY, R.J.H., RAWNSLEY, K. & SANDERSON, D.J. (eds) *Fractured Reservoirs*. Geological Society, London, Special Publications, **270**, 43–53, https://doi.org/10.1144/GSL.SP.2007.270.01.03